# Multichannel Communication based on Adaptive Equalization in Very Shallow Water Acoustic Channels

**Bien Aik TAN [(1)], Mehul MOTANI [(1)], Mandar CHITRE [(2)] and Swee Sen QUEK [(3)]**

(1) National University of Singapore, 21, Lower Kent Ridge Road, Singapore 119077
(2) Acoustic Research Laboratory, National University of Singapore, 12A Kent Ridge Road, Singapore 119223
(3) DSO National Laboratories, 20, Science Park Drive, Singapore 118230

## ABSTRACT

Very shallow water acoustic communication channels are known to exhibit fading due to time-varying multipath arrivals. This is further complicated by impulsive snapping shrimp noise that is commonly present in warm shallow waters. This paper will present a communication channel model simulation for such a channel. The paper also presents results from the use of single-carrier differential phase shift keying (DPSK) modulation which does not require an elaborate method for estimating the carrier phase. The receiver designs in simulation and trial data analysis are based on the least mean square (LMS) adaptive linear equalizer (LE) and decision feedback equalizer (DFE). Multichannel combining and forward error correction (FEC) schemes such as turbo product codes (TPC) are employed to improve performance. We will present performance results based on simulated data as well as for real data collected from the sea.

## INTRODUCTION

Very shallow water acoustic communication channels are known to exhibit fading due to time-varying multipath arrivals. The shallow water acoustic channel is generally characterized as a multipath channel due to the acoustic signal reflections from the surface and the bottom of the sea. Because of wave motion, the signal multipath components undergo time-varying propagation delays, resulting in signal fading. This is further complicated by impulsive snapping shrimp noise that is commonly present in warm shallow waters, such as those around Singapore.

Recently, channel measurements at medium frequency ranges (12.7-24.3kHz) in very shallow water (15-30m) at distances ranging from 1km to 2.7km in the coastal sea of Singapore have indicated that it is possible to reliably send high data rate (~9kbps) communication signals, especially at longer distances (Tan, Quek & Zou 2006).

In this paper, we will present a channel model that simulates the multipath fading characteristics of the shallow underwater channel. We will briefly verify this model by comparing its simulated power delay profiles with actual delay profiles measured from the sea. Next, we will simulate a single carrier DPSK communication with adaptive equalization and compare its performance with the analysed trial data. We will also present the performance of LE-LMS and DFE-LMS adaptive receiver for the sea trial data. Its performance can be further enhanced with multichannel combining and FEC methods such as TPC.

## CHANNEL MODEL

For high frequencies and shallow water, Ray theory is adequate to describe the multipath structure of the channel (Coates 2001). High frequency here refers to having an acoustic wavelength that is smaller than the bottom depth, preferably less than 0.1 of the bottom depth. For this research work, the depth is roughly 30m maximum, the sound velocity is typically 1540m/s and the carrier frequency is typically at 18.5kHz for medium range communication. Thus the wavelength to bottom depth ratio is 2.77 x$10^{-3}$.

Because of the isovelocity assumption (constant sound velocity over depth), the rays here are straight. This is a fair assumption as most sound velocity profiles recorded in our shallow water showed less than 1m/s variation in velocity over depth (Tan 2006). This is reasonable in that the depth is considered shallow giving little variation of temperature over depth, and tidal currents usually established a good mixing of salinity that lead to isovelocity conditions.

Zielinski, Yoon and Wu (1995) proposed a multipath model for shallow waters shown in figure 1. The channel model is characterized by Ray theory (simplified due to constant sound velocity profile and constant bottom depth assumptions) and extending it to a multipath expansion for a series of reflections resulting in multipath arrivals at the receiver.

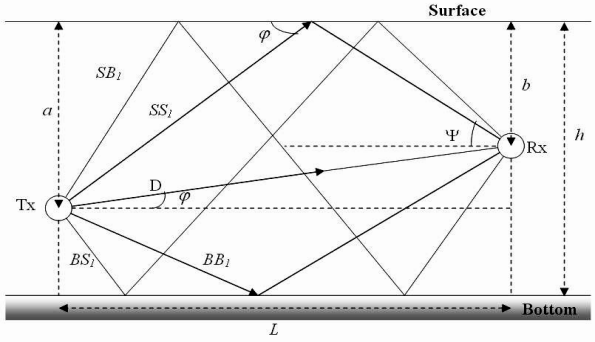


**Figure 1**. Multipath structure of shallow water channel

The surface reflection loss and bottom reflection loss are computed using the Beckmann-Spizzichino model and Rayleigh reflection coefficient respectively (Yeo et al. 2000). Apart from these losses, we also account for spherical spreading loss and frequency dependent volume absorption loss. The transmitted signal path can be classified as direct path D or multipath. Multipaths are classified into four types and order of reflections, $n$. For example, notation $SS_1$ will denote multipath signal which make the first and last boundary re-

flection with the surface with first order of reflection as shown in the figure above. The channel can be visualized using the method of images (Brekhovskikh 1960) to compute the signal path length, angle of arrivals and delays.

Up to this point, our discussions have been on a time-invariant propagation model. However, it is well known that the shallow water channel exhibits time varying multipath fading (Stojanovic 2002). Time variability in the channel response results from a few underwater phenomenon. Random signal fluctuation due to micro-paths (Poor 1998) is one of the phenomenons but it is more dominant in deep oceans where there are stronger presence of internal waves and turbulence (Stojanovic 2002). For all signal paths, micro-paths of each signal path in shallow channels may be due to scattering by small inhomogeneities in the medium and other suspended scatterers. In addition, surface scattering due to surface waves and random Doppler spreading of surface reflected signals due to motion of reflection point could add to the channel's time variability for shallow water.

Chitre (2004; 2006) has made several observations on short range (~50m) variations of individual signal paths. The individual signal path is observed to exhibit approximate Rayleigh fading. To model the correlated time variation, the method from Chitre (2006, p.74) is adopted here where each amplitude of signal path is modeled as Rayleigh random process with a median determined by magnitude of multipath arrival and a time correlation determined by the Doppler spread $W_d$. The time correlation method is detailed in Chitre (2006, Appendix A).

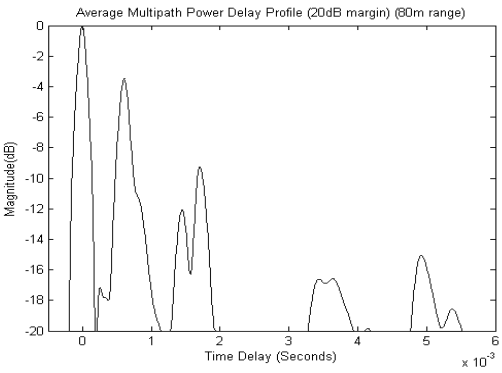


Source: (Tan, Quek & Zou 2006)

**Figure 2**. Average power delay profile from sea trial (80m distance)

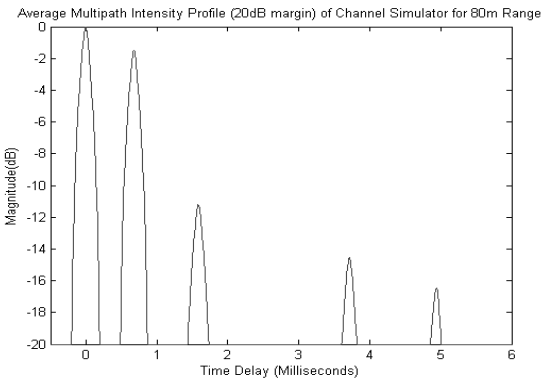


**Figure 3.** Average power delay profile from channel simulator (80m Range)

Figure 2 shows the actual multipath profile measured from a distance of 80m. The transmitter depth and bottom depth was 10m and 16m respectively. The receiver depth and bottom depth was 5m and 17m respectively. We measured the transducer depths by marking our cable every one metre. As there was tidal current swaying the transducer in one direction, actual transducer depths may differ. The simulated transmitter, receiver and bottm depth was 8m, 5.5m and 17m respectively. Figure 3 shows a similar multipath profile plot for a simulated 80m distance. Hence, the channel model was able to replicate a similar multipath structure when compared to the actual channel.

In Tan et. al. (2004), it was noted that low frequency ambient noise in shallow Singapore waters is dominated by shipping and reclamation noise while at higher frequencies; the predominant noise is snapping shrimp noise. A characteristic of snapping shrimp noise is that it is highly impulsive, resulting in a heavy tailed distribution. This implies that the Gaussian distribution, which is commonly used to characterize noise in most environments in communications, is a poor fit for the ambient noise in Singapore waters. This was backed up by data collected in Chitre (2004) and Tan, Quek and Zou (2006) which proposed the use of alpha-stable distribution to characterize the impulsiveness of snapping shrimp noise. The best fit alpha-stable probability density function (PDF) had an alpha of between 1.6 and 1.8 and these yield a much better fit than the Gaussian PDFs. The alpha stable noise generator has been used for communication channel simulation in this paper. Details of alpha stable noise generation can be found in Tan, Quek and Zou (2006).

## SIMULATION

The channel model and a binary DPSK communication system were simulated in MATLAB®. Shown in figure 4 is the DPSK frame format. A synchronisation preamble is inserted before each data frame. The preamble is a differentially encoded 128 or 512 bits m-sequence while the data segment contained 901 bits of differentially encoded pseudo random data.

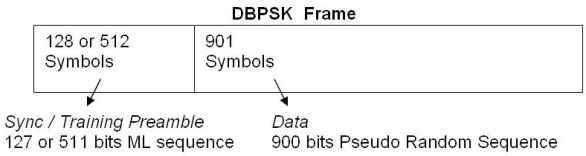


**Figure 4.** DBPSK frame format

**Table 1.** Simulation parameters

| | |
|---|---|
| **Centre Frequency** | 18.5kHz |
| **Symbol Rate** | 9250sym/s |
| **Raised Cosine Filter Alpha** | 0.25 |
| **Oversampling** | 16 |
| **Arbitrary Start Bit** | '1' |

### Processing

The sync data and pseudo random data is differentially encoded as shown below.

$$d(k) = a(k)d(k-1) \tag{1}$$

where $d(k)$ are the differentially encoded bits and $a(k) \in \{\pm 1\}$ is the original bit sequence. The arbitrary start bit is $d(0) = 1$.

The baseband antipodal DPSK frame is raised cosine filtered, upsampled and upconverted to the pass band centre frequency at the transmitter. The signal is then fed into the channel simulator described in the previous section. Geometrics and geophysics parameters of the channel such as transmitter's and receiver's depth, bottom depth, distance, Doppler spread, sound velocity, sea-bottom density and velocity ratios are approximates of actual sea trials that will be pre-

sented in the later part of the paper. This was done for comparison and to indicate how well the channel simulator is able to replicate the effects of shallow water channels.

At the receiver, the carrier was then removed by multiplying the signal by the sine and cosine carriers and passing the signal through a raised cosine filter. Timing recovery and synchronization is then achieved by correlating the filtered signal with the preamble sequences to obtain the best sampling instance. The data sequence was then differentially decoded (equation (2)) and compared with the transmitted sequence to determine the total number of errors, bit error rates (BERs) and frame error rates (FERs). The FER is the ratio of erroneous frames received to the total number of frames received.

$$\tilde{a}(k) = \mathrm{sgn}(\mathrm{Re}[r(k) \times r^*(k-1)]) \quad (2)$$

where *r(k)* is the complex baseband received signal after down conversion and raised cosine filtering. The simulated results are shown in Table 2. This will be compared with the real data analysis in the next section.

**Table 2.** Simulated BER results of binary DPSK in shallow water channels

| Range (m) | SNR (dB) | No. of frames | Error bits | BER | FER |
|---|---|---|---|---|---|
| **80** | 26.8 | 264 | 49915 | 2.10e-1 | 1 |
| **130** | 23.9 | 264 | 62861 | 2.65e-1 | 1 |
| **560** | 25.1 | 264 | 61287 | 2.58e-1 | 1 |
| **1040** | 20.4 | 198 | 59247 | 3.32e-1 | 1 |
| **1510** | 17.1 | 198 | 47448 | 2.66e-1 | 1 |
| **1740** | 17.5 | 198 | 3351 | 1.88e-2 | 1 |
| **2740** | 12.7 | 198 | 1131 | 6.30e-3 | 7.93e-1 |

## EXPERIMENTAL DESCRIPTION

The experiments were conducted in the coastal sea of Singapore. The transmitter was on one ship and the receiver on the other (see Figure 5). An omni-directional medium frequency (resonant at 18.5kHz) projector was used to transmit the signal with a source level of up to 180dB re $1\,\mu Pa$ at 1m (summed from 12.7kHz to 24.3kHz). The receiver was a three band nested linear vertical array of nine hydrophones. In this experiment, we only utilized the 18.5kHz receiving band of 5 hydrophones. For both dry end equipments, we have a portable personal computer (PC) with a National Instrument multi-function data acquisition PCI card. During the sea trial, the receiving ship (ship B), remained at a fixed position while the transmitting ship (Ship A), moved to different locations. The multi-channel received signal was low pass filtered at 50kHz and then acquired at a sampling rate of 200kHz by the receiver PC.

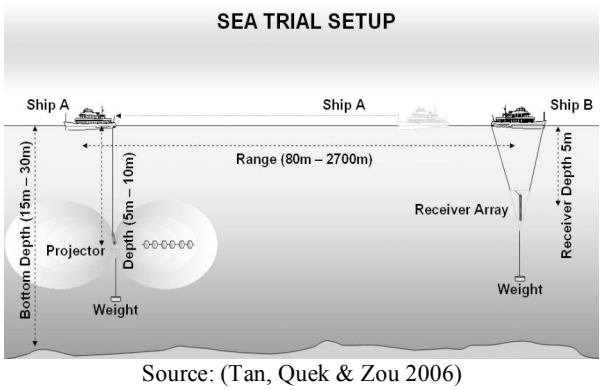


Source: (Tan, Quek & Zou 2006)

**Figure 5.** Experimental set up for channel characterization.

The channel measurements are summarised in the following table 3. For more details, please refer to Tan, Quek and Zou (2006).

**Table 3.** Delay spread and coherence bandwidth results for different ranges

| Range (m) | Root Mean Square (RMS) Delay Spread (ms) | Doppler Spread, $W_d$ (Hz) | Doppler Shift (Hz) |
|---|---|---|---|
| **80** | 1.2 | 9 | -1,+2 |
| **130** | 1.9 | 8 | -1 |
| **600** | 0.85 | 4 | -2 |
| **1030** | 0.85 | 3 | 0 |
| **1510** | 0.38 | 2 | -1 |
| **1740** | 0.13 | 2 | +1 |
| **2740** | 0.10 | 3 | +2 |

Source: (Tan, Quek & Zou, 2006)

### Preliminary DPSK Performance results

For each distance, the DBPSK frames were transmitted from ship A and received at Ship B for a duration of 60 seconds. Each DPSK frame follows the format in figure 4 and table 1.

The baseband antipodal DBPSK frame was raised cosine filtered, upsampled and upconverted to the pass band centre frequency at the transmitter. This signal was pre-prepared in MATLAB® prior to the trial. At shorter distances <1000m, the sync preamble contained 128 bits. At longer distances, the sync preamble contained 512 bits. The reason for the change is the large variation observed in sync pulses at shorter distances and anticipated higher propagation loss at further distances. The m-sequence length was increased in-situ at longer distances to give better processing gain. Channel one at each of the ranges was selected for analysis. The signal was demodulated in the method described in the previous sub-section. The baseband data was then sampled at T/2 intervals and stored in files, where T is the symbol interval. These were done offline in MATLAB® and the SNRs, BER and FER were computed. Table 4 shows the results of the analysis. The trend of decreasing BER as the distance increases or delay spread decreases is also observed, when compared to table 3. One can also note the higher SNR at shorter ranges but the corresponding poor BERs indicate that performance degradation is largely due to strong inter-symbol interference (ISI) and higher Doppler spread measured during the trial.

**Table 4.** Trial BER results of DBPSK in shallow water channels – Channel one

| Range (m) | SNR (dB) | No. of frames | Error bits | BER | FER |
|---|---|---|---|---|---|
| **80** | 28 | 264 | 57391 | 2.41e-1 | 1 |
| **130** | 25.4 | 264 | 81626 | 3.44e-1 | 1 |
| **560** | 26.4 | 264 | 52390 | 2.21e-1 | 1 |
| **1040** | 20.2 | 198 | 59791 | 3.36e-1 | 1 |
| **1510** | 17.4 | 198 | 51465 | 2.89e-1 | 1 |
| **1740** | 17.4 | 198 | 2047 | 1.15e-2 | 9.90e-1 |
| **2740** | 12.0 | 198 | 1681 | 9.43e-3 | 9.85e-1 |

Plotting the BERs of table 2 and table 4 into figure 6, we compare the BERs of the trial and simulated data for each distance. Overall, if the BER points lie near the diagonal it meant that the BERs of the simulated and trial data are correlated. Our simulation BERs were shown to be correlated to the BERs of the trial data. The 'grey' data set are for the next segment in which adaptive equalization were used to compensate for the ISI and to improve the BER performance.

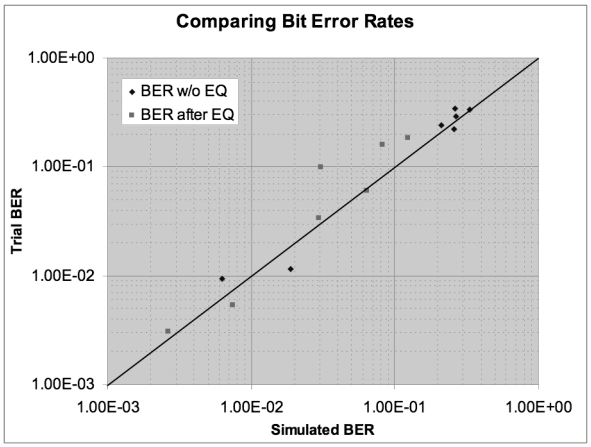


**Figure 6** Comparing BERs of trial and simulated data for the same distance.

## ADAPTIVE EQUALIZATION

Shallow water channels are known for their multipaths, fading and ISI effects (Stojanovic 2002). Without equalization or diversity techniques, achievable data rates remains very low. In order to have high data rates, adaptive equalization can be applied to compensate for the fading and ISI effects. The combinations of linear or non-linear equalization and coherent detection have been investigated extensively. However, there are comparatively fewer studies on combined equalization and non-coherent detection, although such receivers are less complex and more robust against carrier phase variation.

Linear equalizer and decision feedback (Proakis 2001, Chap 11) type of equalizers have been employed in the analysis of simulated and trial data. (See figures 7 and 8).

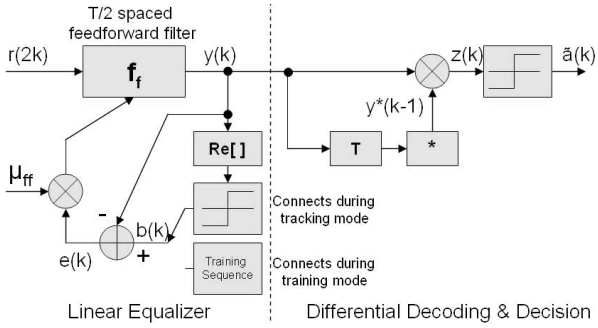


**Figure 7.** Linear equalizer

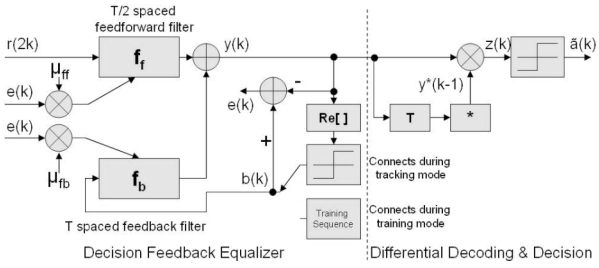


**Figure 8.** Decision feedback equalizer

Note that fractionally spaced equalizers (Treichler, Fijalkow & Johnson 1996) were used in the analysis. The inputs to the equalizers were T/2 spaced because the signal bandwidth, after raised cosine filtering, is about 11.5kHz and the baud rate is 9250 symbol/second. In order to allow the equalizer to compensate for the distortion, sampling must be done above Nyquist rate. Thus, a T/2 sampling rate gives an effective sampling rate of 18500 sample/seconds that is adequate for 11.5kHz broad baseband signal.

Most of the adaptive equalization for non coherent DPSK signals based their error signal between the differentially decoded soft-output and the decision output or $e(k) = \tilde{a}(k) - z(k)$ from figure 7 and 8 (Stojanovic 2005; Robert, Wolfgang & Johannes 2001). We note that the error signal based on differentially decoded output may contain unnecessary higher levels of *e(k)* as a bit error in the *y(k)* will give twice the bit errors in differential decoding. This will in turn cause unnecessary filter taps adjustment even though the current detected bit in *y(k)* may be correct. On the contrary, we take the error signal between the differentially encoded training signal and the filter output or $e(k) = d(k) - y(k)$ during training and $e(k) = \text{sgn}(\text{Re}[y(k)]) - y(k)$ during tracking.

They are mainly two sets of adaptive algorithms: one is the least mean square (LMS) and its variants and the other is recursive least square (RLS) and its variants. Though the RLS converges much faster than the LMS algorithm, it has a higher complexity than the LMS. In addition, the LMS algorithm may be more stable than the RLS algorithm. Hence, we chose LMS algorithm for our analysis. Below are summaries of LMS algorithm for LE and DFE.

### Summary of LE-LMS Algorithm

Input: $\mathbf{f}_f(k)$ Feed forward filter tap coefficient vector
$\mathbf{r}(2k)$ Input vector at 2/T sampling rate
*b(k)* Training signal / tracking signal
$\mu_{ff}$ Feed forward tap adaptation step size (0.04)
N – No. of feed forward filter taps (129)
$k^{th}$ iteration
Output: *y(k)* Filter output at T sampling rate
$\mathbf{f}_f(k+1)$ Feed forward tap coefficient vector update

**1. Filtering:**

$$\mathbf{r}(2k) = \left[r(2k+\tfrac{N-1}{2})\ r(2k+\tfrac{N-2}{2})\ \ldots r(2k)\ldots\ r(2k-\tfrac{N-2}{2})\ r(2k-\tfrac{N-1}{2})\right]^{\mathrm{T}} \quad (3)$$

$$\mathbf{f}_f(k) = \left[f_0\ f_1\ \ldots\ldots f_{N-1}\right]^{\mathrm{T}} \quad (4)$$

$$y(k) = \mathbf{f}_f(k)^{\mathrm{T}} \times \mathbf{r}(2k) \quad (5)$$

**2.Reference Signal:**

During training $\Rightarrow\ b(k) = d(k)$ (6)

During tracking $\Rightarrow\ b(k) = \text{sgn}(\text{Re}[y(k)])$ (7)

**3.Error Estimation:**

$$e(k) = b(k) - y(k) \quad (8)$$

**4.Tap Coefficient Adaptation:**

During training $\Rightarrow\ \mathbf{f}_f(k+1) = \mathbf{f}_f(k) + \mu_{ff} e(k)\mathbf{r}^*(k)$ (9)

During tracking $\Rightarrow\ \mathbf{f}_f(k+1) = \mathbf{f}_f(k) + \frac{\mu_{ff}}{4} e(k)\mathbf{r}^*(k)$ (10)

### Summary of DFE-LMS Algorithm

Input: $\mathbf{f}_f(k)$ Feed forward filter tap coefficient vector
$\mathbf{f}_b(k)$ Feed back filter tap coefficient vector
$\mathbf{r}(2k)$ Input vector at 2/T sampling rate
$\mathbf{b}(k-1)$ Feed back vector at T sampling rate
*b(k)* Training signal / Tracking signal
$\mu_{ff}$ Feed forward tap adaptation step size (0.04)
$\mu_{fb}$ Feed back tap adaptation step size (0.004)
$N_f$ – No of feed forward filter taps (65)

$N_b$ – No of feed back filter taps (64)
$k^{th}$ iteration

Output: $y(k)$ Filter output at T sampling rate
$\mathbf{f}_f(k+1)$ Feed forward tap coefficient vector update
$\mathbf{f}_b(k+1)$ Feed back tap coefficient vector update

**1. Filtering:**

$$\mathbf{r}(2k) = \left[r(2k+N-1)\ r(2k+N-2)\ ...r(2k)\right]^{\mathrm{T}} \quad (11)$$

$$\mathbf{f}_f(k) = \left[f_0\ f_1\ .....f_{N_f-1}\right]^{\mathrm{T}} \quad (12)$$

$$\mathbf{b}(k) = \left[b(k-1)\ b(k-2)\ ...b(k-N_b)\right]^{\mathrm{T}} \quad (13)$$

$$\mathbf{f}_b(k) = \left[f_0\ f_1\ .....f_{N_b-1}\right]^{\mathrm{T}} \quad (14)$$

$$y(k) = \left(\mathbf{f}_f(k)^{\mathrm{T}} \times \mathbf{r}(2k)\right) + \left(\mathbf{f}_b(k)^{\mathrm{T}} \times \mathbf{b}(k)\right) \quad (15)$$

**2.Reference Signal:**

During training $\Rightarrow$ $b(k) = d(k)$ (16)

During tracking $\Rightarrow$ $b(k) = \mathrm{sgn}(\mathrm{Re}[y(k)])$ (17)

**3.Error Estimation:**

$$e(k) = b(k) - y(k) \quad (18)$$

**4.Tap Coefficient Adaptation:**

During training $\Rightarrow$ $\mathbf{f}_f(k+1) = \mathbf{f}_f(k) + \mu_{ff} e(k)\mathbf{r}^*(k)$ (19)

$$\mathbf{f}_b(k+1) = \mathbf{f}_b(k) + \mu_{fb} e(k)\mathbf{b}^*(k) \quad (20)$$

During tracking $\Rightarrow$ $\mathbf{f}_f(k+1) = \mathbf{f}_f(k) + \frac{\mu_{ff}}{4} e(k)\mathbf{r}^*(k)$ (21)

$$\mathbf{f}_b(k+1) = \mathbf{f}_b(k) + \frac{\mu_{fb}}{2} e(k)\mathbf{b}^*(k) \quad (22)$$

## LE-LMS Performance in Simulation

The simulated data set that was analysed in Table 2 was used to assess the LE-LMS performance. The results are tabulated in table 5. All the BERs have been reduced due to equalization when compared to table 2.

**Table 5.** Simulated BER results of DBPSK in shallow water channels after LE

| Range (m) | SNR (dB) | No. of frames | Error bits | BER | FER |
|---|---|---|---|---|---|
| **80** | 26.8 | 264 | 19688 | 8.29e-2 | 1 |
| **130** | 23.9 | 264 | 29361 | 1.24e-1 | 1 |
| **560** | 25.1 | 264 | 15262 | 6.42e-2 | 1 |
| **1040** | 20.4 | 198 | 5305 | 2.98e-2 | 9.90e-1 |
| **1510** | 17.1 | 198 | 5488 | 3.08e-2 | 9.19e-1 |
| **1740** | 17.5 | 198 | 468 | 2.63e-3 | 5.96e-1 |
| **2740** | 12.7 | 198 | 1326 | 7.44e-3 | 7.88e-1 |

The ensemble average mean square error (MSE) of *e(k)* over all the frames at 1040m are calculated and shown in figure 9(a). It shows the equalizer has converge to its minimum sum squared error (MMSE). Figure 9(b) shows the tap weight adaptation results showing the estimated impulse response of the inversed channel for one of the frames. Figure 9(c) shows the differential decoding results if no processing was done on the input signal *r(k)*. Black crosses indicate the known data bit of '0' and grey circles indicate known data bit of '1'. Improvements are seen in the in-phase quadrature (IQ) plot (figure 9(d)) after linear equalization.

## LE-LMS Performance in Trial

Similarly, we applied LE-LMS onto the trial data to compare it with the simulated ones. And the results are shown in table 6. Both their BERs in table 5 and table 6 are plotted in figure 6. It shows that their results are approximately correlated and both witness the same trends of decreasing BER with increasing distance. All these also agree with the results in channel measurements of Tan, Quek and Zou (2006).

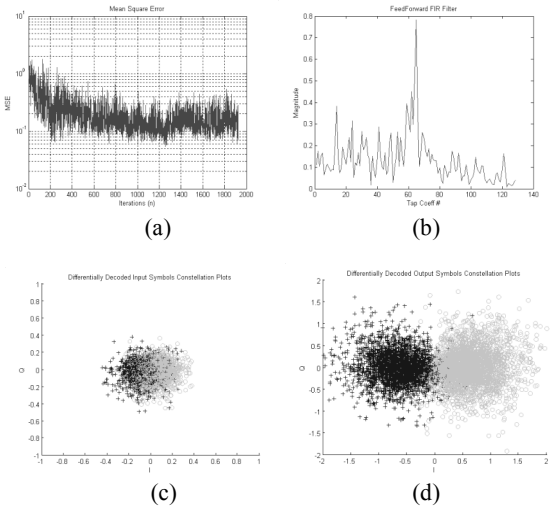


**Figure 9.** Simulated linear equalization-distance: 1040m (a) Mean square error (b) Filter tap coefficients (c)Input I-Q plot of differential decoded *r(k)* (d) Output I-Q plot of $\tilde{a}(k)$

**Table 6.** Trial BER results of DBPSK in shallow water channels after LE– Channel one

| Range (m) | SNR (dB) | No. of frames | Error bits | BER | FER |
|---|---|---|---|---|---|
| **80** | 28 | 264 | 37647 | 1.58e-1 | 1 |
| **130** | 25.4 | 264 | 43316 | 1.82e-1 | 1 |
| **560** | 26.4 | 264 | 14457 | 6.04e-2 | 1 |
| **1040** | 20.2 | 198 | 6024 | 3.38e-2 | 1 |
| **1510** | 17.4 | 198 | 17561 | 9.85e-2 | 1 |
| **1740** | 17.4 | 198 | 542 | 3.04e-3 | 6.46e-1 |
| **2740** | 12.0 | 198 | 955 | 5.36e-3 | 8.39e-1 |

The mean squared error, tap weights and IQ plots for the trial 1040m data set are plotted in figure 10. Note the similarities in the plots when compared to figure 9. Figure 9(a) does converge the same way as figure 10(a). In addition, both their lower bounds which indicate its MMSE is also approximately the same. The difference in plots of figure 9(b) and figure 10(b) is normal as the estimates for each frame will be different due fading.

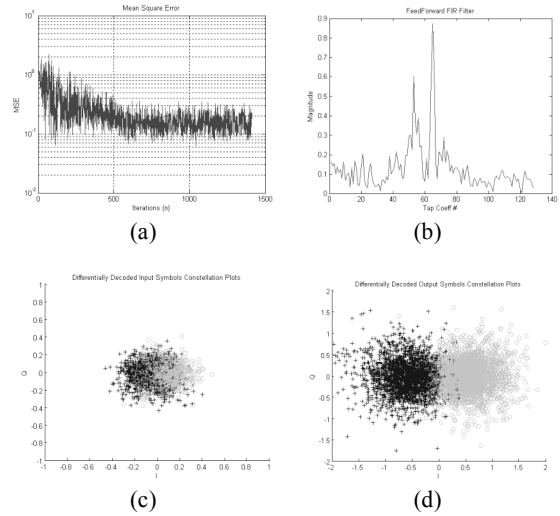


**Figure 10.** Linear equalization on trial data-distance: 1040m (a) Mean square error (b) Filter tap coefficients (c) Input I-Q plot of differential decoded *r(k)* (d) Output I-Q plot of $\tilde{a}(k)$

These have shown that the channel simulator is a good approximation of the actual trial channel. The focus of this paper will now shift its attention to improving the performance of real data. It will begin with analysing the trial performance of DFE-LMS and then, compare it with the LE-LMS ones to determine which is better.

### DFE-LMS Performance in Trial

Similarly, we applied DFE-LMS onto the trial data. And the results are shown below in table 7.

**Table 7.** Trial BER results of DBPSK in shallow water channels after DFE– Channel one

| Range (m) | SNR (dB) | No. of frames | Error bits | BER | FER |
|---|---|---|---|---|---|
| **80** | 28 | 264 | 54051 | 2.27e-1 | 1 |
| **130** | 25.4 | 264 | 67754 | 2.85e-1 | 1 |
| **560** | 26.4 | 264 | 37531 | 1.58e-1 | 1 |
| **1040** | 20.2 | 198 | 12929 | 7.26e-2 | 1 |
| **1510** | 17.4 | 198 | 18250 | 1.02e-1 | 1 |
| **1740** | 17.4 | 198 | 188 | 1.06e-3 | 4.24e-1 |
| **2740** | 12.0 | 198 | 881 | 4.94e-3 | 8.79e-1 |

In general the BERs for distances less than 1500m of the DFE-LMS performed poorer than the LE-LMS (see figure 14). These are due to the poor input BERs for distances less than 1500m that resulted in more detected bits errors to propagate down the feedback filter giving, rise to higher mismatch in channel inversion. On the other hand, if the BER improves as in 1700-2700m, the bit errors in the feedback filter decreases resulting in better estimate to counter post ISI effects. Then the advantage of DFE kicks into effect by reducing noise feedback and feedback only bit energy. This noise feedback is inherent in LE as post samples (bit energy and noise) remained in the filter to equalize the present sample. Evidently, this can be seen in table 6 and table 7 or figure 14 where the DFE BER performance is better than that of LE at longer distances. However, an equalizer that can perform reasonably well at all distances was preferred and we chose the LE over the DFE to further enhance the BER performance. In the next segment, multichannel combining with LE was introduced to further reduce the BERs.

## MULTICHANNEL COMBINING

All five channels in the nested array were LE, combined by summation and differentially decoded as shown in figure 11 and their BER results are tabulated in table 8. It shows BER reductions at all distances (see figure 14).

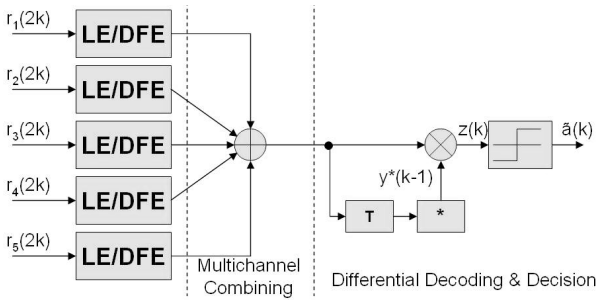


**Figure 11.** Multichannel combining method with LE or DFE

Figure 12 shows the effect of multichannel combining in decreasing the BER. This is evident by comparing the IQ plots figure 12(d) and figure 12(e).

At all distances, the bit errors, BERs and FERs have been reduced (see figure 14 and figure 15). The next segment will show the channel coding performance of trial data. We will combine LE, MC and channel coding to produce reliable communications.

**Table 8.** Trial BER results of DBPSK in shallow water channels after LE and MC

| Range (m) | SNR (dB) | No. of frames | Error bits | BER | FER |
|---|---|---|---|---|---|
| **80** | 28 | 264 | 6237 | 2.62e-2 | 9.77e-1 |
| **130** | 25.4 | 264 | 19441 | 8.18e-2 | 1 |
| **560** | 26.4 | 264 | 4241 | 1.78e-2 | 9.85e-1 |
| **1040** | 20.2 | 198 | 543 | 3.05e-3 | 7.63e-1 |
| **1510** | 17.4 | 198 | 7304 | 4.10e-2 | 1 |
| **1740** | 17.4 | 198 | 210 | 1.18e-3 | 4.49e-1 |
| **2740** | 12.0 | 198 | 161 | 9.03e-4 | 4.24e-1 |

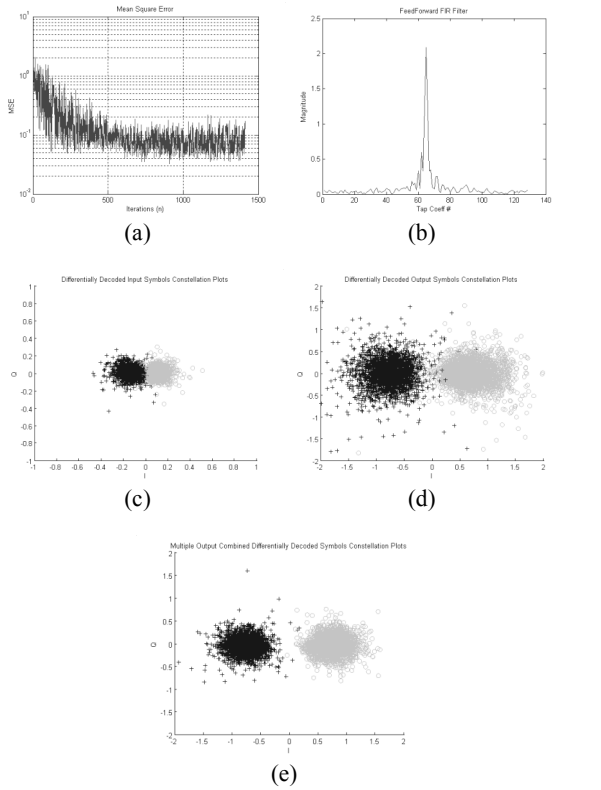


**Figure 12.** Multichannel combining with linear equalization-distance: 2740m (a) Mean square error (b) Filter tap coefficients (c)Input I-Q plot of differential decoded *r(k)* (d) single channel output I-Q plot of $\tilde{a}(k)$ (e) Multiple channel combined IQ Plot

## CHANNEL CODING

Turbo codes and the associated iterative decoding techniques have generated much interest within the research community in recent years for their ability to achieve an exceptionally low BER with a signal to noise ratio per information bit close to Shannon's theoretical limit on a Gaussian channel (Berrou & Glavieux 1996). Turbo Product Codes (TPC) were selected as the FEC due to their powerful error-correction capability based on soft-input-soft-output (SISO) iterative decoding algorithm and their excellent BER performance at high code rate (> 0.65) (Pyndiah 1998). Implementation-wise, TPCs are less complex than Berrou's turbo convolutional codes, with the Chase Algorithm simplifying the decoding effort required for TPCs (Chase 1972).

The TPC encoder structure is illustrated in figure 13. For TPC encoding, a total of 676 information bits are placed into a $k \times k$ array. Then a single-parity-check code is applied to every row of the array to result in a $k \times n$ matrix and subse-

quently the same code is applied to every column of the resultant matrix to yield an $n \times n$ matrix that contains 900 bits (a so-called product code). The code rate is $k^2/n^2 \approx 0.75$. For DBPSK modulation, each OFDM frame contains just one TPC code block.

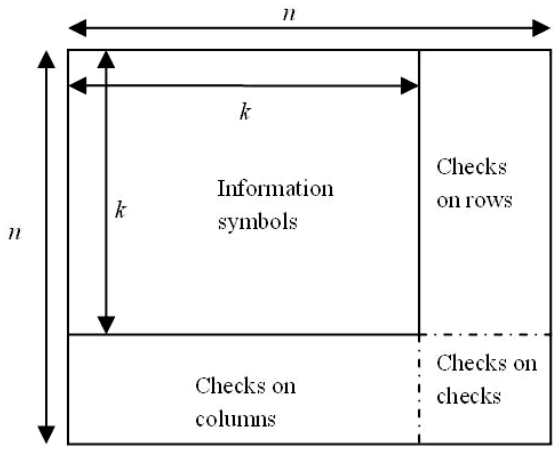


**Figure 13.** Turbo product code (TPC) encoder structure

The TPC decoding is based on soft-input soft-output iterative algorithms and the details can be found in Pyndiah (1998).

Although the data in the DPSK frame format is uncoded, the channel effect encountered in the received trial data can be extracted from the combined *y(k)* in figure 11 and ported over to a TPC codeword. This was done by the following method on the data segment of *y(k)*:

1. Channel effect extraction

$$c_e(k) = \frac{y(k)}{d(k)} \tag{23}$$

2. Porting channel effect to differentially encoded TPC codeword $d_c(k)$

$$y_c(k) = d_c(k) c_e(k) \tag{24}$$

where $d_c(k) = a_c(k) d_c(k-1)$ and $a_c(k)$ is the TPC codeword.

This is done assuming that:

$$y(k) = d_y(k) e^{j\theta} + n(k) \tag{25}$$

where $d_y(k)$ is the scaled version of $d(k)$, $\theta$ is the single value constant phase offset and $n(k)$ is the noise. This is done for all the distances' data set and their BERs and FERs have been computed and found to be the same as the original data in table 8, as expected. The coding performance are computed and tabulated in Table 9.

Figures 14 and 15 give an overview on the performance enhancements over the different schemes applied. Finally, with LE, MC, and TPC, more than 75% of the frames received were error free at most distances. At distances of 1040m, 1740m and 2740m, all coded frames received were 99%-100% recovered with no errors. The performance of 140m and 1510m were considered poor. These may be caused by the multipath structures with deep frequency selective fading which the equalizer cannot compensate.

**Table 9.** Trial BER results of DBPSK in shallow water channels after LE, MC and TPC

| Range (m) | No. of frames | Error bits | BER | FER |
|---|---|---|---|---|
| **80** | 264 | 2006 | 1.12e-2 | 1.74e-1 |
| **130** | 264 | 14356 | 8.04e-2 | 7.12e-1 |
| **560** | 264 | 476 | 2.67e-3 | 6.06e-2 |
| **1040** | 198 | 0 | <7.47e-6 | <5.05e-3 |
| **1510** | 198 | 1831 | 1.37e-2 | 2.58e-1 |
| **1740** | 198 | 0 | <7.47e-6 | <5.05e-3 |
| **2740** | 198 | 5 | 3.75e-5 | 5.05e-3 |

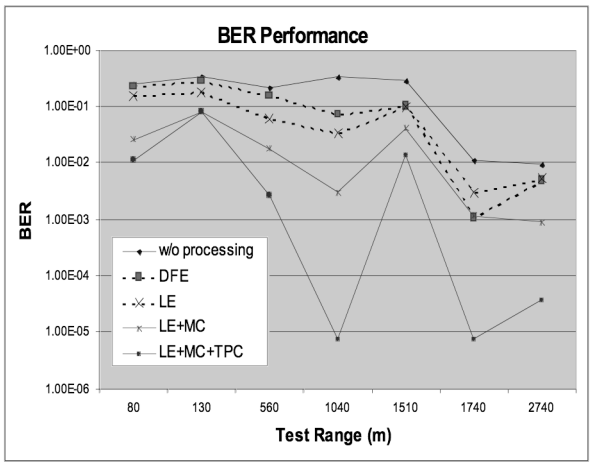


**Figure 14.** BER performances of different schemes

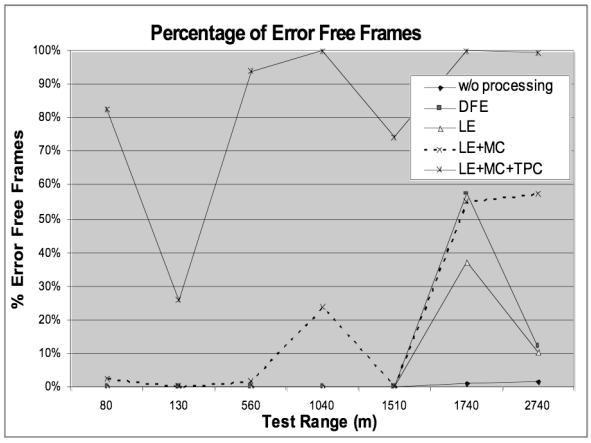


**Figure 15.** Error-free frame performances of different schemes

## CONCLUSION

This paper has presented a communication channel model simulation for the shallow water channel environment. The BERs of a simulated and sea-trial DPSK communication system have validated that the channel simulator is a good approximation to the real shallow water channel. It is noted that the performance of the adaptive linear equalizer (LE) is generally better than the decision feedback equalizer (DFE) for most distances. Multichannel combining has been employed and found to have improved BER performance satisfactorily. Forward error correction (FEC) scheme such as turbo product codes (TPC) are employed to improve performance by removing correctable errors and increasing the number of error free frames. With the combined use of linear equalization, multichannel combination and turbo decoding, we see a substantial improvement in data reliability in terms of BERs and error free frames recovered.

## ACKNOWLEDGEMENT

We would like to thank DSO National Laboratories for making the datum available. In addition, we would like to thank Mr Koh Tiong Aik and Mr Zhong Kun for their help with the sea trial experiments and data transmissions/acquisitions.

## REFERENCES

Berrou, C & Glavieux, A October 1996, 'Near optimum error correcting coding and decoding: turbo codes', *IEEE Transactions on Communications*, Vol.44, Issue 10, pp. 1261-1271.

Brekhovskikh, LM 1960, *Waves in Layered Media*, 1st ed., Academic Press, New York.

Chase, D January 1972, 'Class of algorithms for decoding block codes with channel measurement information', *IEEE Transactions on Information Theory*, Vol.18, Issue 1, pp.170-182.

Chitre, M, Potter, JR & Ong, SH November 2004, 'Underwater Acoustic channel characterization for medium-range shallow water communications', *MTS/IEEE Proceedings of TECHNO-OCEANS Conference '04*, Vol:1, pp40-45,.

Chitre, M 2006, 'Underwater Acoustic Communications in Warm Shallow Water Channels', P.hD. Thesis, Singapore: National University of Singapore.

Coates, R 2001, *The Advanced SONAR Course*, Seiche.com, United Kingdom.

Poor, HV & Wornell, GW 1998, *Wireless Communications - Signal Processing Perspective*, Prentice Hall Signal Processing Series, USA.

Proakis, JG 2001, *Digital Communications*, 4th ed., McGraw Hill, USA-New York.

Pyndiah August 1998, 'Near-optimum decoding of product codes: block turbo codes', *IEEE Transactions on Communications*, Vol.46, Issue 8, pp.1003-1010.

Robert, S, Wolfgang HG & Johannes BH May 2001, 'Adaptive Linear Equalization Combined with Noncoherent Detection for MDPSK Signals', *IEEE Transactions on Communications*, Vol. 48, No.5 pp. 733-738.

Stojanovic, M 2002, *Underwater Acoustic Digital Signal Processing and Communication Systems, Kluwer*, USA.

Stojanovic, M September 2005, 'An Adaptive Algorithm for Differentially Coherent detection in the Presence of Intersymbol Interference', *IEEE Journal on Selected Areas in Communications,* Vol. 23, No.9, pp. 1884-1890.

Tan, BA 2006, 'Underwater Acoustic Communications', M.Eng. Thesis, Singapore: National University of Singapore – Dissertation in progress.

Tan, BA, Quek, SS & Zou, N May 2006, 'Characterization of Multipath Acoustic Channels in very Shallow Waters for Communications', *Proceedings of the 1st Oceans Asia Pacific Conference 2006*, IEEE, Singapore.

Tan, SP, Koay, TB, Venugopalan, P, Chitre, M & Potter, JR April 2004, 'Development of a shallow water ambient noise database', *International Symposium on Underwater Technology 2004,* pp.169-173, Taiwan.

Treichler, JR, Fijalkow, I & Johnson, Jr CR May 1996, 'Fractionally Spaced Equalizers-How long should they be?', *IEEE Signal Processing Magazine*, pp.65-81.

Yeo, HK, Sharif, BS, Adams, AE & Hinton, OR September 2000, 'Analysis of Experimental Shallow Water Network Channel and Theoretical Channel Model', *Proceedings of the Oceans 2000 Conference*, Vol.3 Pg.2025-2029.

Zielinski, A, Yoon, YH & Wu, L October 1995, 'Performance Analysis of Digital Acoustic Communication in a Shallow Water Channel', *IEEE Journal of Oceanic Engineering*, Vol:20 Issue 4, pp. 293-299.